Scanning Microscopy

Volume 1996
Number 10 *The Science of Biological Specimen Preparation for Microscopy*
Article 8

4-24-1996

Imaging Molecular Structure of Channels and Receptors with an Atomic Force Microscope

Ratneshwar Lal
University of California, Santa Barbara, rlal@sbphy.physics.ucsb.edu

Scanning Microscopy Supplement 10, 1996 (pages 81-96) 0892-953X/96$5.00+.25
Scanning Microscopy International, Chicago (AMF O'Hare), IL 60666 USA

IMAGING MOLECULAR STRUCTURE OF CHANNELS AND RECEPTORS WITH AN ATOMIC FORCE MICROSCOPE

Ratneshwar Lal

Neuroscience Research Institute, University of California, Santa Barbara, CA 93106,

(Received for publication October 10, 1995 and in revised form April 24, 1996)

Abstract

Biological membranes contain specialized protein macromolecules such as channels, pumps and receptors. Physiologically, membranes and their constituent macromolecules are the interface surfaces toward which most of the regulatory biochemical and other signals are directed. Yet very little is known about these surfaces. The structure of biological membranes has been analyzed primarily using imaging techniques that are limited in their resolution of surface topology. An atomic force microscope (AFM) developed by Binnig, Quate and Gerber, can image molecular structures on specimen surfaces with subnanometer resolution, under diverse environmental conditions. Also, AFM can manipulate surfaces with molecular precision: it can nanodissect, translocate, and reorganize molecules on surfaces. The surface topology has been imaged for several hydrated channels, pumps and receptors which were a) present in isolated native membranes, b) reconstituted in artificial membrane or, c) expressed in an appropriate expression system. These images, at molecular resolution, reveal exciting new findings about their architecture. AFM induced "force dissection" reveals surfaces which are commonly inaccessible. In whole cell studies, in addition to the molecular structure of membrane receptors and channels, correlative electrical and biochemical activities have been examined. Such study suggests a "single cell" experiment where the structure-function correlation of many cloned channels and receptors can be understood.

Key Words: Scanning force microscopy, Biomolecular imaging, Quaternary structure, Imaging receptors and channels, gap junctions, porins, acetylcholine receptor, vacuolar ATPase, bacteriorhodopsin, cholera toxin.

*Address for correspondence:
R. Lal
Neuroscience Research Institute,
University of California
Santa Barbara, CA 93106,
Telephone number: 805-893-2350
FAX number: 805-893-2005
E-mail: rlal@sbphy.physics.ucsb.edu

Introduction

Currently, molecular structures of channels and receptors are being studied primarily by electron microscopy, electron and X-ray diffractions, and infra-red spectroscopy. Molecular functions, on the other hand, are being examined using various biochemical, electrophysiological and molecular biological techniques. However, it is difficult, if not impossible, to combine both structure and function studies with these techniques, mainly because the techniques used for structural studies require an unfavorable operating environment and an extensive sample preparation which limits the functional states of biological macromolecules. Moreover, these techniques provide very little information about the surfaces of channels and receptors, the very sites of molecular interaction.

An atomic force microscope (AFM) (Binnig *et al.*, 1986) can image the three-dimensional (3D) surface structure of a wide variety of biological specimens (for reviews see Lal and John, 1994; Hansma and Hoh, 1994, Yang and Shao, 1995). AFM can image, at molecular resolution, native samples bathed in an aqueous medium. This provides the opportunity of observing biochemical and physiological processes in real time at molecular and often atomic level and thus can be used for direct molecular structure-function studies of membrane channels and receptors. In addition, AFM is uniquely qualified to provide topographical information of the surfaces to which most of the regulatory biochemical and other signals are directed. Other microscopical techniques such as the scanning electron microscope (SEM) can also view surfaces. However, unlike SEM, AFM can image in an aqueous environment and often at a greater resolution. AFM, due to its significantly greater signal-to-noise ratio, can provide an accurate measure of long-range packing such as crystallinity even for a small cluster of particles (for example, 20 x 20 particles).

AFM has been used to image a wide variety of individual biological macromolecules, whole cells, membranes and membrane-bound proteins, and a few interactive processes (for review see Lal and John, 1994). We have recently imaged ion channels in a)

native membranes such as gap junctions (Hoh *et al.*, 1991; Lal *et al.*, 1995b), b) reconstituted membranes such as porin channels (Lal *et al.*, 1993), and c) expressed in *Xenopus* oocyte such as acetylcholine receptors (AChR) (Lal and Yu, 1993). Our development of membrane *force dissection* (Hoh *et al.*, 1991, Lal *et al.*, 1995a) suggests that the commonly inaccessible regions can be imaged. Dynamic biochemical processes such as enzyme-substrate reactions, crystal growth and protein polymerization, and physico-chemical properties such as elasticity, viscosity and various chemical forces of biological specimen have been studied (Drake *et al.*, 1989; Durbin *et al.*, 1993; Florin *et al.*, 1994; Shroff *et al.*, 1995). In addition, an AFM can be used as a nanomanipulator (for nanodissection and for force-induced changes in molecular conformations; Hoh *et al.*, 1991; Lal *et al.*, 1995a; Muller *et al.*, 1995) as well as an exquisite sensor of molecular forces - hydrogen bonds, Van der Waals and electrostatic forces (for review, see Lal and John, 1994).

Principle of Operation

For a detailed treatise on the principle of operation, resolution, and limitations of AFM, see Lal and John, 1994.

Briefly, an AFM image consists of a series of parallel line contours obtained by scanning the surface of a specimen placed on a xyz translator across a molecularly sharp tip with a small ($\sim$ a nanoNewton (nN)) tracking force. The tip is mounted on a microcantilever with a small spring constant. As the tip is scanned, the net interaction force between the molecules on probe tip and sample surface deflects the tip and hence the cantilevered spring. The deflection is sensed by detecting the angular deflection of a laser beam reflected off the back of the mirrored cantilever, which is converted to electrical signals by photodetectors. An electronic feedback loop keeps the cantilever deflection and hence the tracking force constant by moving the sample up and down as the tip traces over the contours of the surface (Figure 1). An image is obtained by plotting the vertical motion (z) of the xyz translator and hence the sample height (z) as a function of specimen lateral position (xy).

Recent improvements in AFM imaging include the "Tapping mode imaging" (Hansma *et al.*, 1994a) and combined light fluorescence, laser confocal and atomic force microscopes (Hansma *et al.*, 1994b; Hillner *et al.*, 1995; Lal *et al.*, 1995a,b). In the tapping mode imaging, the lateral force of interaction is significantly reduced and a considerably greater lateral resolution has been achieved on imaging isolated biological macromolecules. The inverted microscope based dual fluorescence and force microscope (Figure 1) allows simultaneous multimodal imaging and the stationary sample stage facilitates the ease of combining other electrophysiological and biochemical techniques for correlational studies.

Two major factors for the AFM to be applicable to biological imaging are:

a) Resolution: With AFM, the images are formed by reconstructing the contour of the interaction forces between the probe and the specimen. By selecting a small imaging area and appropriate operating conditions, one can distinguish adjacent structures less than a nanometer apart as the signal-to-noise ratio in an AFM image is sufficiently large compared to EM and other techniques. For hard crystals such as calcite, atomic resolution is obtained (Ohnesorge and Binnig, 1993). For soft biological specimens such as a living cell, the resolution is reduced (for review, see Lal and John, 1994). In biological specimens with a high density of protein and limited mobility such as membranes with channels and receptors, however, the resolution could be comparable to that for a hard crystal. On many biological membranes including gap junctions, Na^+-K^+ ATPase, AChR, bacteriorhodopsin and porin channels, a subnanometer resolution has been obtained (see below).

b) Identity of the imaged structures; correlative studies: Though AFM could provide, with molecular resolution, surface information of crystalline as well as amorphous materials, it is often difficult to identify the nature of individual components, especially if the surface contains a heterologous population of structures. This is often the case with most of the biological membranes, except in favorable systems like purified native gap junctions (Lal *et al.*, 1995b), purple membrane bacteriorhodopsin (Butt *et al.*, 1990; Muller *et al.*, 1995) and reconstituted channels and receptors (porins and cholera toxins (Lal *et al.*, 1993; Mou *et al.*, 1995). The suitability of using the AFM for biological imaging will rely on an unambiguous identification of imaged structures. For mixed macromolecules, critical comparisons obtained from AFM and alternative/complementary techniques, such as structural probes of EM and X-ray diffraction, biochemical and immunological binding assays (Figures 2,3), pharmacological labeling and electrophysiological measurements will be essential (Lal *et al.*, 1995b; Lal and Yu, 1993; Kordylewski *et al.*, 1994; Bustamante *et al.*, 1995; Han *et al.*, 1995; Arakawa *et al.*, 1992; for review see Lal and John, 1994).

Kordylewski *et al.* (1994) have reported an elegant correlative study between AFM and the transmission electron microscopy (TEM). They examined freeze fractured replicas of adult rat atrial tissue by both TEM and AFM (Figure 2). The same replicas were analyzed and the same details were identified which allowed a critical comparison of surface topography by both

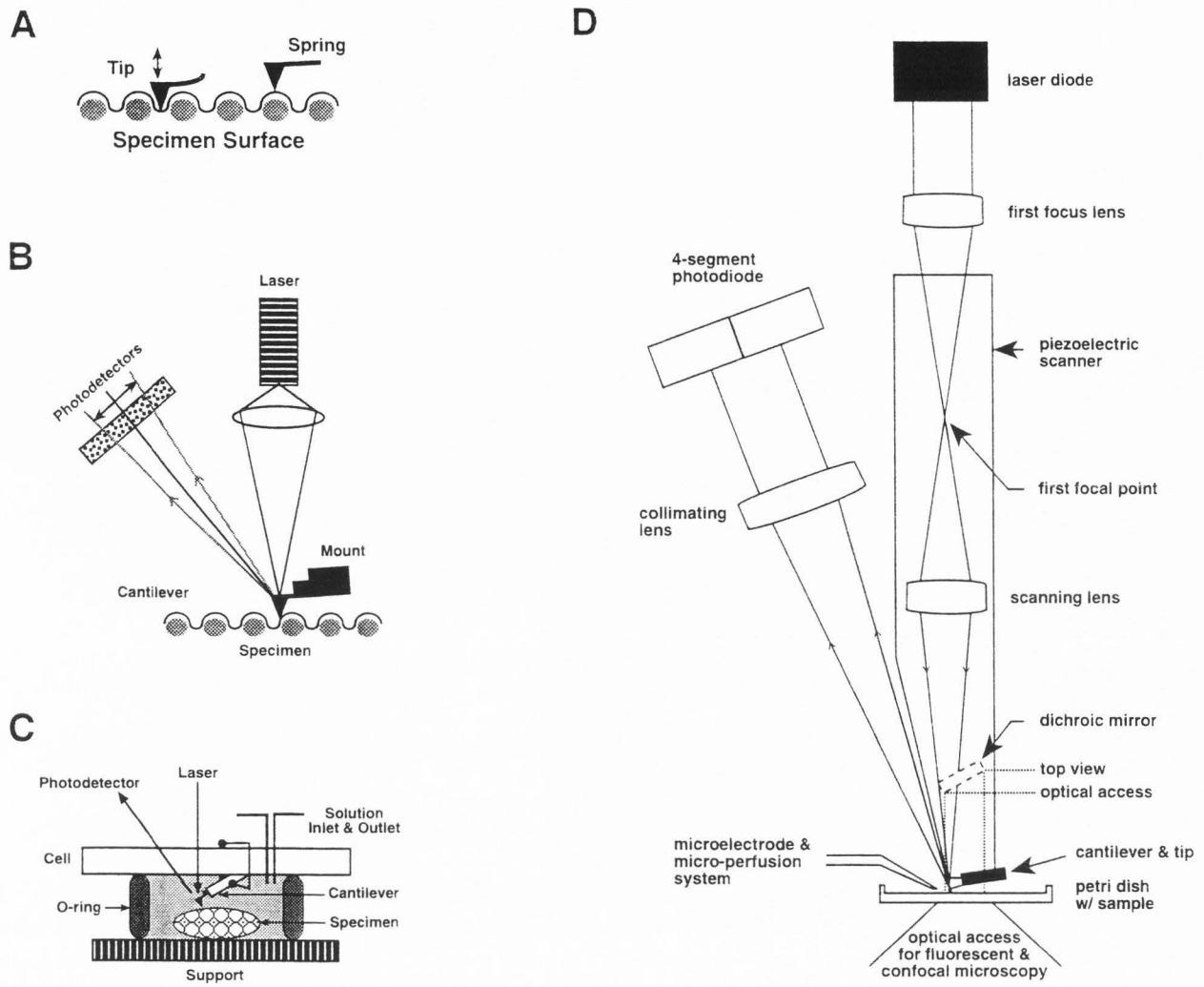

Figure 1: Schematics of operating principle of an AFM. **A**. Force sensor for an AFM. The force sensor is a spring deflection system consisting of a sharp tip micro fabricated onto a cantilever spring with a small spring constant. As the tip scans the specimen surface, the interaction forces between the tip and specimen deflect the tip and hence the cantilever. The deflection equivalent to the interactive forces (as a function of tip-surface separation) is used to create 3-D surface topography. **B**. An optical deflection detection system, which is the most commonly used. A cantilever deflection reflects the incident collimated laser beam. The reflected beam is incident asymmetrically on position sensitive photo detectors. The output of these detectors is used in a feedback loop to keep the deflection (and hence the force) constant while the tip scans the specimen. **C**. An AFM with a fluid cell. Both the cantilevered tip and the specimen are immersed in a fluid. The surface of the fluid cell is transparent and has two openings for fluid inlet and outlet. **D**. A schematic diagram of the optical component of a combined light fluorescence and force microscope. The first focal point is located inside the upper portion of the piezoelectric scanner. After the positions of the lenses are adjusted, the scanning focused spot accurately tracks the cantilever and the zero-deflection signal from the 4-segment photodiode is independent of position within the scan area. One of the key advantages of the new AFM is that there is optical access to the sample from above and below. Thus the new AFM can be combined with an optical microscope of high numerical aperture. The other key advantage is that since the sample is stationary during scanning and can be large, techniques for on-line perturbations and recordings can easily be incorporated. (For details, see Lal and John, 1994, and Hansma *et al.*, 1994b).

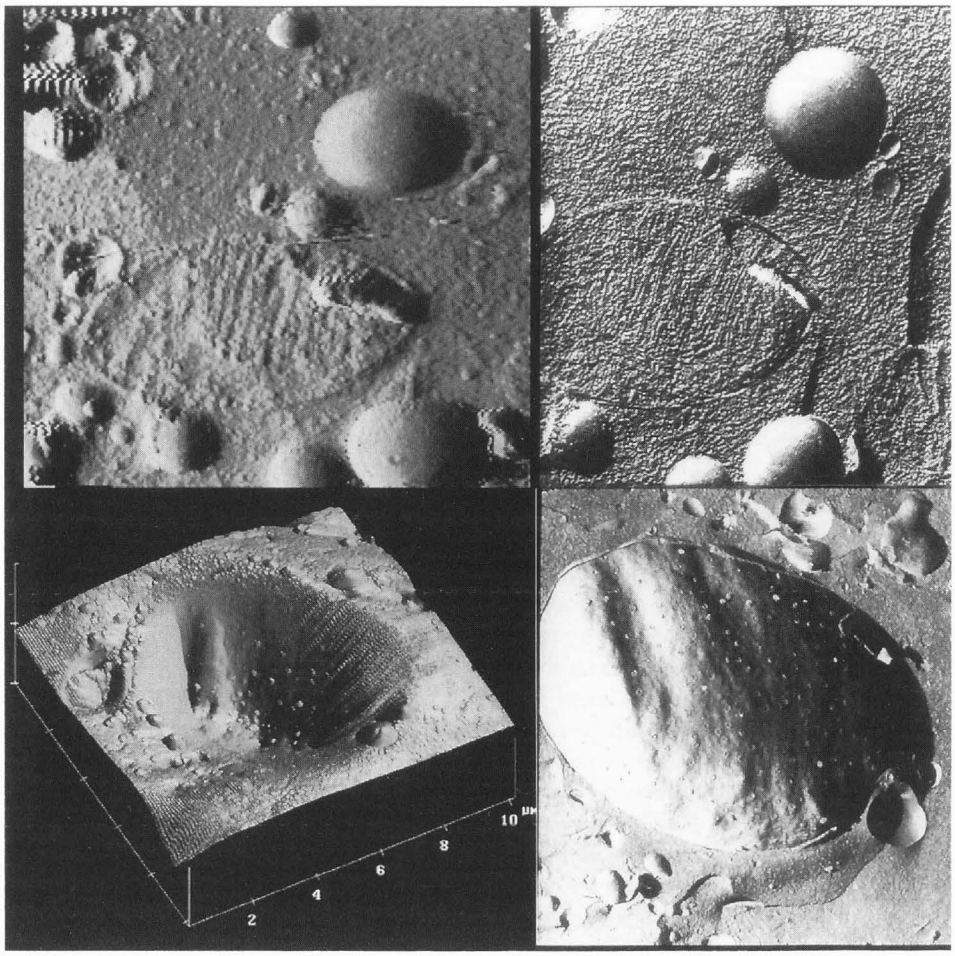

Figure 2: Comparison of the same structural details in a freeze-fracture replica of a rat cardiac tissue imaged with AFM (left) and TEM (right). Top: atrial granules and mitochondrion with cristae; bottom: a cell nucleus with pores in the nuclear envelope. (for details see Kordylewski *et al.*, 1994).

techniques. AFM images of large scale subcellular structures (nuclei, mitochondria, granules) correlated well with those from the TEM. However, AFM images of smaller features and surface textures appeared somewhat different from TEM images. This presumably reflects the difference in the surface sensitivity of the AFM vs TEM, as well as the nature of images in AFM (3D surface contour) and TEM (2D projection). In addition, AFM images provided new information about the replica itself. Unlike TEM, it was possible to examine both sides of the replica with AFM; the resolution on one side was significantly greater compared to the other side. It was also possible to obtain quantitative height information which is not readily available with TEM.

The simple design of AFM allows it to be integrated with other techniques, such as fluorescence and laser confocal microscopies (Hillner *et al.*, 1995; Lal *et al.*, 1995b; Figure 3). This can permit an independent verification with appropriately labeled markers: first use fluorescent signals to identify specific areas and then use atomic force imaging to obtain the ultrastructural details. We have imaged purified cardiac gap junctions that were labeled with anti-Cx43 antibody (Figure 3). All fluorescently labeled regions when imaged by AFM showed gap-junctional plaque-like features. In this preliminary study, as our goal was simply to locate all the membranes that were gap junction specific, we had used a considerably large amount of antibodies which covered the entire membrane, resulting in the net increase of ~ 5 nm in membrane height. Antibodies adsorbed to the glass substrate alone had a similar height variation. Thus, it is feasible to obtain molecular resolution structural information on membrane proteins present singly and in small clusters as long as they have detectable immunofluorescence signals.

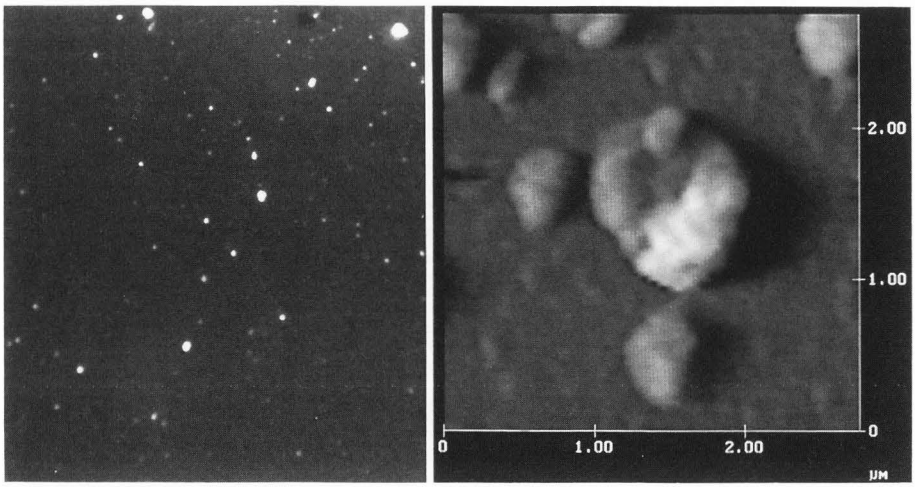

Figure 3: Left: Fluorescence image of anti-Cx43 labeled gap junctions. Right: AFM image of gap junctions in the same field of view which showed fluorescence labeling (for details see Lal *et al.*, 1995b).

Sample Preparation

The atomic force microscope can be used to image specimens in both aqueous and dry conditions, at ambient temperature and pressure. Imaging conditions influence the choice of substrate, the stability of the specimen with respect to its interaction with the probe and the preservation of the specimen with respect to its physiological or biochemical functions.

The physico-chemical characteristics of the sample and sample-support interactions determine or suggest ways under which it can be imaged. Problems encountered can merely be as simple as getting the sample to attach to the support. Techniques can include the drying down of samples and adsorption against specially prepared surfaces. Low sample-support interaction requires that low forces be used for imaging or the tip essentially sweeps the sample from the support. Originally, graphite (HOPG hydrophobic uncharged), mica (hydrophilic negatively charged) and glass were the supports most routinely used. These supports can also be modified chemically to adjust their hydropathicity, charge density, and their polarity. Today the repertoire has expanded greatly.

It is possible to modify or coat the support such that it can act as a ligand for the sample and thus orient the specimen in a defined way. It is also possible to use artificial systems to generate constraints where there were none before. One such elegant study is that of Yang *et al.* (1993) who incorporated the cholera toxin into synthetic phospholipid bilayers followed by covalent cross-linking. The pentameric structure of the B-subunit was clearly visible. This approach may prove to be widely applicable to other isolated membrane proteins.

Simple adsorption in the presence of appropriate counterions or cross-linking of the membrane fragments to a chemically modified substratum (such as covalent linking) is the most commonly used sample preparation for membrane-bound proteins Karrasch *et al.*, 1993; Yang *et al.*, 1993; Mou *et al.*, 1995). However, such method may not be suitable to observe structural changes *in situ*. For double bilayer membranes such as gap junctions and reconstituted vesicles and planer bilayers, they nevertheless, can leave the upper portions of the proteins free for conformational changes in response to on-line perturbations.

A novel sample preparation system for imaging living cells consists of having a suction pipette hold single cells. By this approach Hörber *et al.* (1992) showed the vaccinia virus leaving a kidney cell. Recently, Hörber *et al.* (1995) have adsorbed membrane patches to the tip of a glass patch pipette and imaged the surface morphology and its modification as a function of the applied force.

Representative Examples

Purified membranes

Gap junctions and hemi-junctions: Proteins that are naturally embedded within membranes and form 2-D crystalline arrays have been examined unfixed and under appropriate buffers. High resolution images of the extracellular face of liver gap junctions show a typical hexameric packing of gap junction channels (connexons?) with pore like indentations (Hoh *et al.*, 1991, 1993). Similar observations were made with cardiac gap junctions (Lal *et al.*, 1995b).

The gap junction channels consist of two hemichannels (connexons), one arising from each plasma membrane. Our AFM images present evidence of hemiplaques in purified heart gap junctions samples (Figure

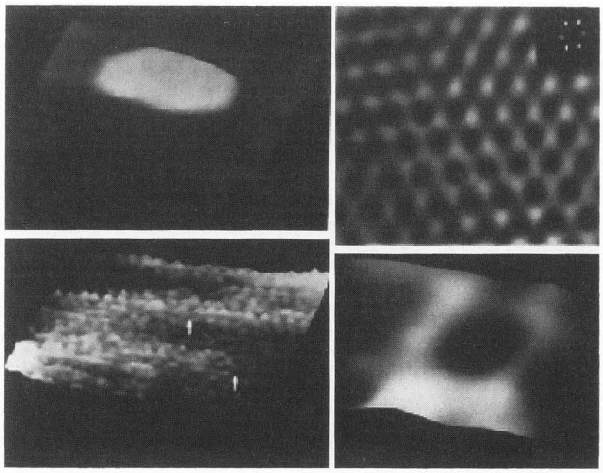

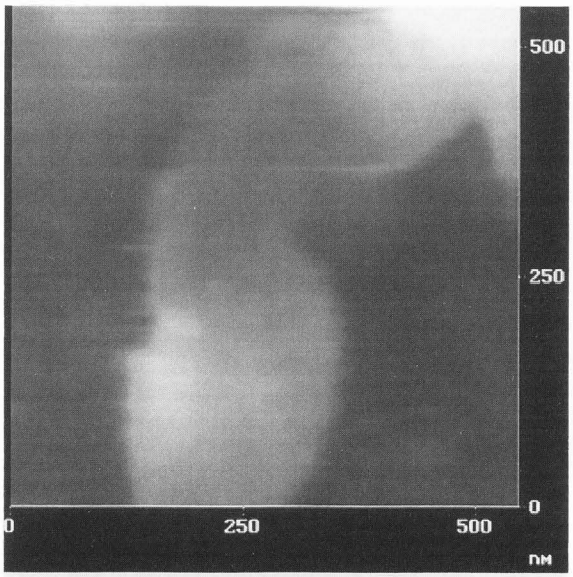

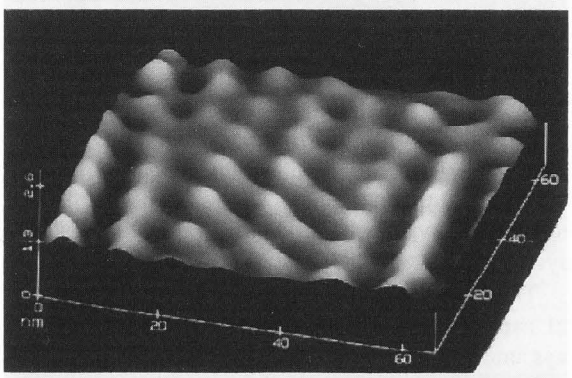

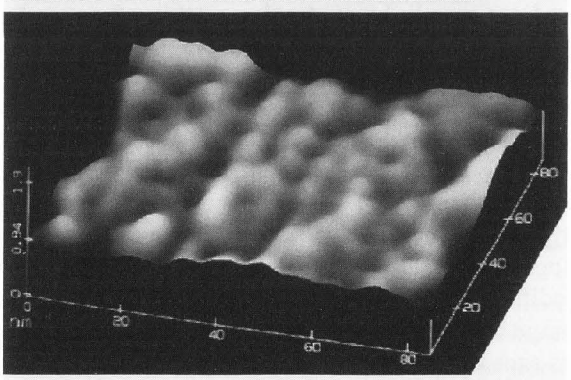

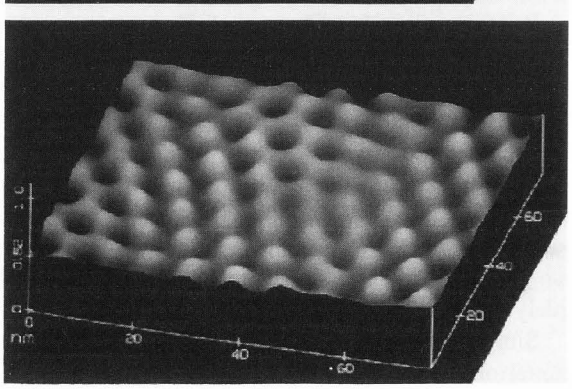

Figure 4: Images of hemi-gap junctions in 30% dextrose solution. Top left: Low magnification surface view image. The scan size is 0.9 x 0.9 μm^2. The thickness of membrane is about 9.6 nm. Bottom left: Medium resolution (scan size 130 x 130 nm^2) surface view image showing arrays of particles which presumably constitute connexons (arrows). The images in Figures A and B are unfiltered. Top right: Inverse Fourier transformed, top view image of another scan area showing a hexagonal long-range packing of connexons with a center to center spacing about 9.7 nm. Bottom right: High resolution (scan size 10 x 10 nm^2) surface view image of a single connexon. Subunits (1-1.5 nm diameter) and a funnel shaped central pore with the outer diameter of abour 2.5 nm are visible. Number of subunits (5 or 6) is difficult to distinguish as reported for liver gap junctions (Hoh *et al.*, 1993). For details see Lal *et al.* (1995b).

Figure 5 : AFM images of vacuolar proton pumps (V-H^+-ATPases). Purified acidosomes were imaged dry or in PBS. Top panel: membranes typical of the purified acidosome fraction. They appear to be collapsed vacuoles, typically <0.5 μm in diameter. Wet imaging. Second panel from the top: Inverse 2D FFT filtered image of the outer surface (presumably, cytoplasmic). A hexagonal long-range packing of proteins with central pore-like depressions is visible. The center-to-center spacing of these pores are ~ 12.8 nm. Dry imaging. Second panel from the bottom: Low pass filtered image of the integral portion of the acidosomes. The head-, and stalk- portions of the acidosomes were biochemically dissected. Structures with central pore-like depression enclosed by proteins with uneven protrusions are apparent. Wet imaging. Bottom panel: Inverse 2D FFT filtered image of the integral portion showing a hexagonal long-range packing. Wet imaging.

4) (Lal *et al.*, 1995b). These samples were characterized by SDS PAGE, thin section EM and negative staining. We have characterized these as hemiplaques based on their thickness (~7-11 nm), as compared to whole junctions (~ 22-25 nm); the presence of subunits with a ~10 nm center-to-center spacing; and the quasi-crystalline hexagonal subunit packing. These dimensions are in close agreement with those determined by high resolution EM. Hemi-plaques comprised ~17-18 % of all plaques imaged and were independent both of sample treatment (trypsinization, and glutaraldehyde fixation) and of imaging conditions (dry, PBS, and 30% dextrose solution). At higher resolution, we were able to delineate individual connexons and subunit structures, showing a central depression ~1.5-2.8 nm in diameter, perhaps representing a pore, and the surrounding 5-6 subunits with an overall diameter of ~6 nm.

It is noteworthy that recent electrophysiological, molecular and immunocytological studies indicate the presence of individual hemichannels in the plasma membrane, though their clustering in plaque-like structure is unclear. Hemichannels, in native plasma membranes, would have to remain closed during normal condition for the cell viability or permselectivity. The role of hemichannels in single cells could be related to the exchange of molecules between the cytoplasm and the extracellular region, regulation of cell volume and programmed cell death. Alternately, the putative hemiplaques may simply be an intermediate stage of junction formation, or it may be the breakdown product.

Purple membrane: Purple membrane has been imaged with an AFM in Several experimental conditions. Molecular resolution images of purple membrane show a three fold symmetry suggesting a trimeric arrangement of bacteriorhodopsin molecules (Butt *et al.*, 1990; Muller *et al.*, 1995a,b). Subunit structure and a force-induced conformational changes have also been reported. These two membrane proteins have been extensively characterized by alternative techniques such as EM. The results from AFM studies are in remarkable agreement with those of negative stain EM images.

One advantage of using AFM for membrane imaging is that the membrane polarity (extracellular vs cytoplasmic surface) could be made unambiguously. For example, a double bilayer gap junction will always have a cytoplasmic surface facing upward. The other advantage is a more precise measurement of the membrane thickness. Such measurement was used to directly and easily distinguish single bilayer vs double bilayer gap junction structures, an observation further confirmed by Nanodissection of the upper layer of the gap junctions (Lal *et al.*, 1995b; Hoh *et al.*, 1991). For purple membranes the thickness measured was substrate dependent, an interesting and important observation that may reflect

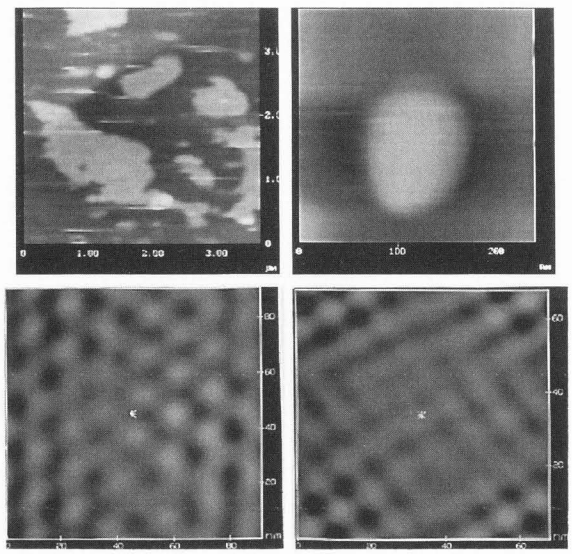

Figure 6: Images of DMPC vesicle morphology and reconstituted OmpF porins for different protein-to-lipid ratios. The protein concentration was kept constant and the lipid concentration was changed ($\mu g/\mu g$) such that the lipid-to-protein (L/P ratio) varied from 0.2 to 2.0. Top left: Vesicles with L/P ratio of 0.2. The vesicles are large and irregular. Top right: A vesicle with L/P ratio of 2.0. The vesicle is small and oval. Bottom left: Inverse 2-D FFT filtered image of porin channels on the upper surface of a vesicle with a L/P ratio of 0.2. Porins appear to be arranged in a long-range hexagonal order. Bottom right: Inverse 2-D FFT filtered image of porin channels on the upper surface of a vesicle with a L/P ratio of 2.0. Porins appear to be arranged in a long-range rectangular order.

---

as yet uncharacterized tip-sample-substrate interactions.

HPI layer: Karrasch *et al.* (1993) have imaged, in buffer, the hexagonally packed intermediate layer (HPI layer) of *D. radiodurans* covalently linked to derivatized glass. At low magnification, flat single membrane layers were visible. These layers consist of doughnut-shaped units which are packed in a hexagonal arrangement. Interestingly, HPI layers were not previously amenable to AFM imaging in buffer without covalent immobilization on a solid substrate. In the present study, the resolution was further improved during repetitive scanning of the same region, though it is unlikely that there was a force-induced rearrangement.

Na^+,K^+-ATPase: Paul *et al.* (1994) have obtained molecular resolution images of Na^+,K^+-ATPase present in purified canine kidney membranes. Imaging under dry condition but using the "tapping mode" of imaging, they reported a channel-like structure with a central pore in the middle of each macromolecule on the cytoplasmic

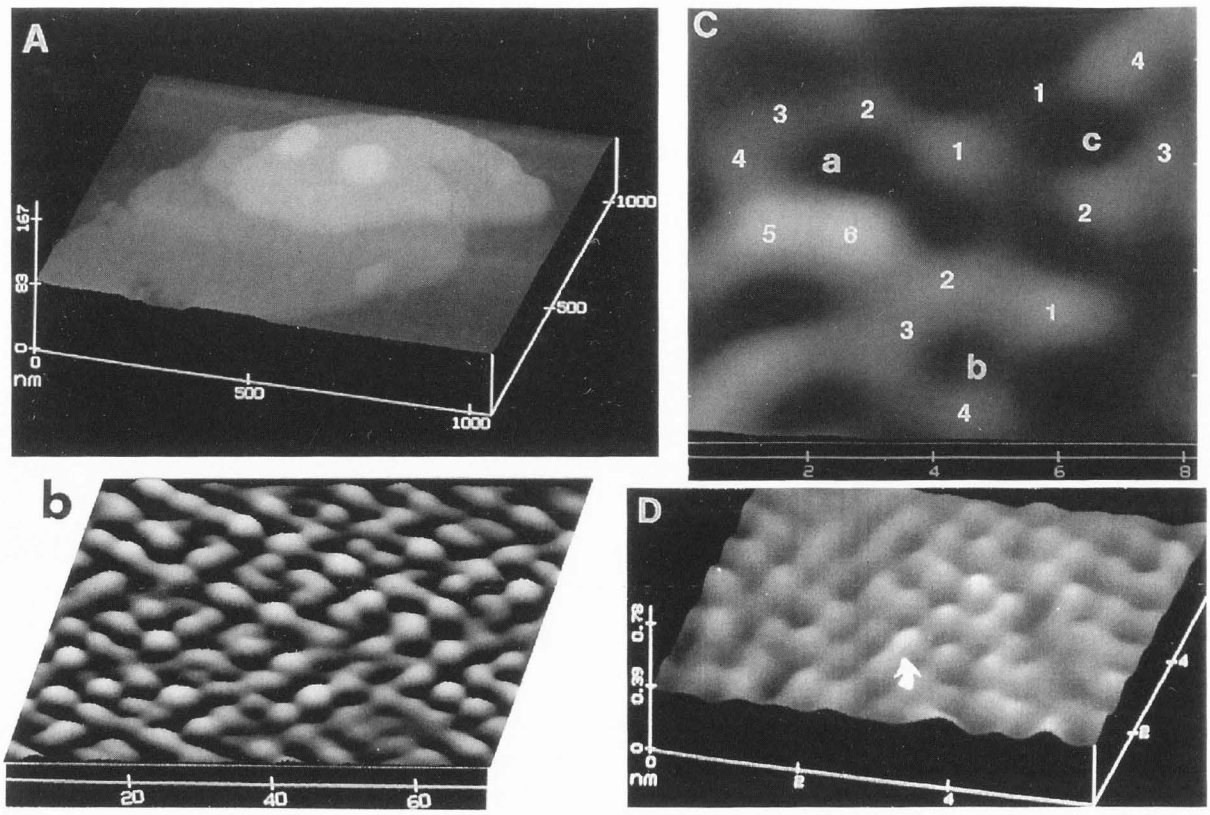

Figure 7: Reconstituted porin channels imaged with an AFM. **A**. Reconstituted DMPC lipid vesicles imaged in PBS. Note, the overlapping multilammelar vesicles. **B**. Inverse 2-D FFT filtered image of *Bordetella pertussis* porin channels reconstituted in DMPC vesicles and imaged under PBS with an AFM. The raw image showed identical pattern but was noisy. Note that the long-range packing is rectangular. Unit cell (~7.9 x 13.8 nm) shows two trimers. The lattice parameters are similar to that reported by EM study. **C**. Subnanometer resolution **unfiltered** image (in 3-D) showing the fine structures in the individual monomers. Note several "bead"-like structures and asymmetrically located pores (marked a,b,c). **D**. Subnanometer resolution images of reconstituted DMPC vesicles without any protein added. Only the filtered image is shown although a similar pattern was visible in the raw data. Individual phospholipid headgroups (~0.5 nm in size; arrowhead) appear to be arranged in a crystalline fashion. For details see Lal *et al.*, 1993.

face of the isolated membranes. The pore diameter ranged from 0.6 -2 nm for a range of different sample treatments. Additionally, in the regions where the protein macromolecules were absent, they were able to see individual lipid head structures with an orthorhombic lattice.

Vacuolar proton pumps (V-H^+-ATPase): Vacuolar proton pumps (V-H^+-ATPase) present in *Dictyostelium discoideum* have been imaged in our laboratory. The acidosomes were isolated and biochemically characterized by Nolta *et al.* (1991). They have previously reported (Nolta *et al.*, 1991) that these vacuolar proton pumps are made of eight subunits, two polypeptides constituting the integral portion while the other six polypeptides are peripheral. Based on the analogy with V-H^+-ATPases of other species, it was proposed that the head-portion consists of two polypeptides, each as three catalytic and three regulatory subunits, and four other polypeptides making the stalk. The V-H^+-ATPase appears to be distinct from either the F_1F_2-type or the E_1E_2-type ATPases.

Figure 5 shows AFM images of V-H^+-ATPase in purified acidosomes. Top panel shows a typical membrane which appeared to be a collapsed vacuole and resembles the previous EM images (Nolta *et al.*, 1991). We were unable to obtain molecular resolution on head-portion of isolated acidosomes while imaging in an aqueous medium. However, on fixed and air-dried membranes, we obtained a higher resolution (~6 nm) on the head-portion of the outer (presumably, cytoplasmic) surface. In some areas of membranes, V-H^+-ATPases were highly packed and as shown in the second panel from the top they were arranged in a hexagonal order with a center-to-center spacing of ~13 nm. Nolta

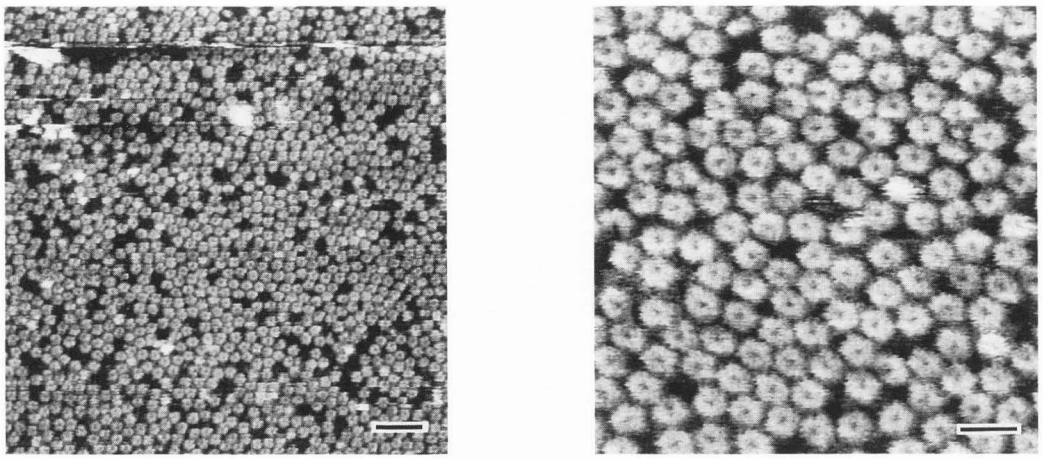

Figure 8: AFM images of individual cholera toxin B-oligomers which were bound to the gangliosides in a bilayer made of egg-PC by the vesicle fusion method. The full coverage of the bilayer is achieved with 10 mol% GM1. Left panel: medium resolution image of the reconstituted bilayer in the gel phase. Scale bar = 30 nm. Right panel: High resolution image. The image quality is comparable to that for the gel-phase image (left side) suggesting that the fluidity of the bilayer did not seriously reduce the resolution in AFM images. B-oligomers with both 6-fold and 5-fold symmetries are visible. Missing subunits are also visible in some B-oligomers. Scale bar = 10 nm. (For details, see Mou *et al.*, 1995).

---

et al. (1991) have previously reported from their EM studies, polygonal particles ~12-13 nm in size with a 3-fold rotational symmetry and suggested that they represent the head portion of the whole V-H^+-ATPase.

After biochemical dissection of the V-H^+-ATPase (Nolta *et al.*, 1991), we were able to obtain a higher resolution (~3 nm), while imaging in an aqueous medium, on the remaining integral portion of V-H^+-ATPase. The bottom two panels show arrangement of individual ATPases. The surface appears to have a fluctuation in height of subunits perhaps reflecting variable extra-membranous protrusions of subunits forming the integral portion. These ATPases were spaced ~13 nm apart. A highly processed image (bottom panel) shows their hexagonal packing. Further detailed studies will be required to determine the correspondence of each head portion to their integral counter part. Such study is feasible by first imaging the whole membrane (and thus imaging the head portion), force-dissecting the head and stalk portions and then imaging the integral portion.

Reconstituted channels and receptors

AFM imaging is not confined to native membranes only. Examples have already been given of using synthetic membranes to provide order to embedded proteins, a technique that may prove beneficial for imaging proteins that do not ordinarily form extended arrays. Membrane proteins forming 2-D arrays in artificial systems have also been imaged.

OmpF porin: Bacterial porins are one of the best studied channel forming membrane proteins. Recently, a number of these porins reconstituted as 2-D crystals into DMPC lipid vesicles were imaged in a fluid environment. For OmpF porins reconstituted in DMPC vesicles, Lal *et al.* (1993) reported that these vesicles assume flattened, double bilayer configurations and also provided support for the 2-D crystal porins (Figures 6,7) (Lal *et al.*, 1993). Often, multilammelar vesicles with incremental step membrane thicknesses were apparent. Molecular resolution images show the predicted trimer formation of porins: similar to that shown by X-ray crystallography and EM reconstruction. Their long range packing was dependent on the lipid-to-protein ratio. OmpF porins showed a mixed hexagonal and rectangular packing, the center to center spacing was consistent with the X-ray diffraction study and the mixed patterns correlate well with the given protein to lipid ratio (0.7).

We undertook a systematic study of the protein-to-lipid interaction and its role in vesicle formation and the regularity of protein packing. Results from our preliminary observation are shown in Figure 6. When the protein-to-lipid ratio was changed from 0.5 to 5.0 (by reducing the lipid concentration while keeping the protein concentration constant), the shape and size of the vesicles changed from very large and irregular to small and spherical. In addition, the packing of proteins changed from hexagonal to rectangular.

Recently, Schabert *et al.* (1995) were able to resolve fine-details of OmpF porins which were reconstituted in DMPC vesicles at a protein-to-lipid ratio of 2.0.

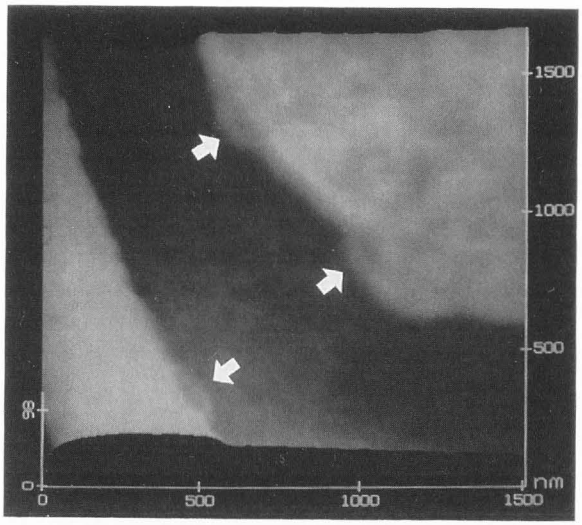

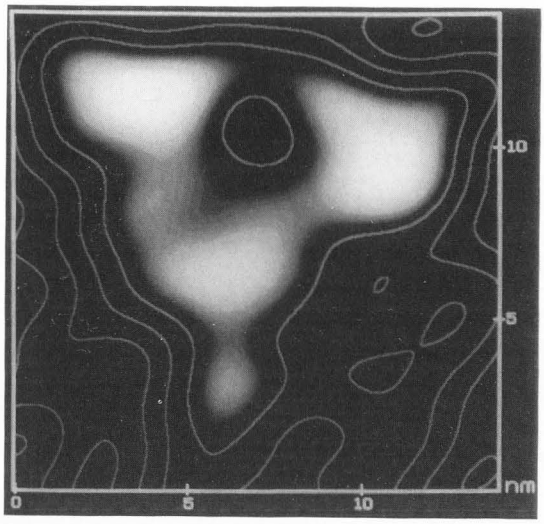

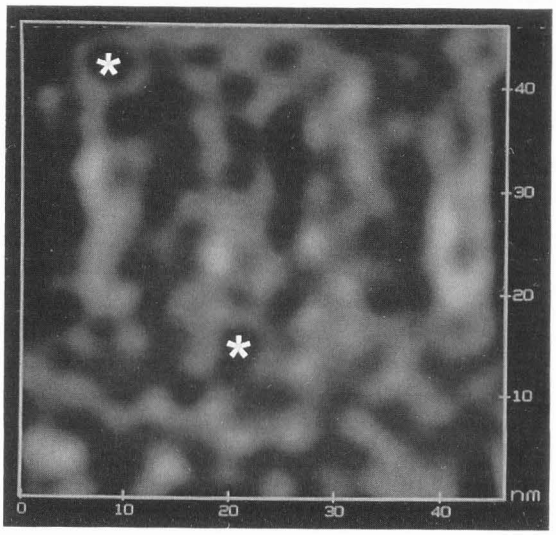

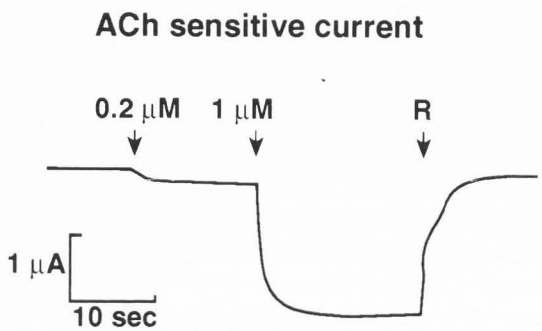

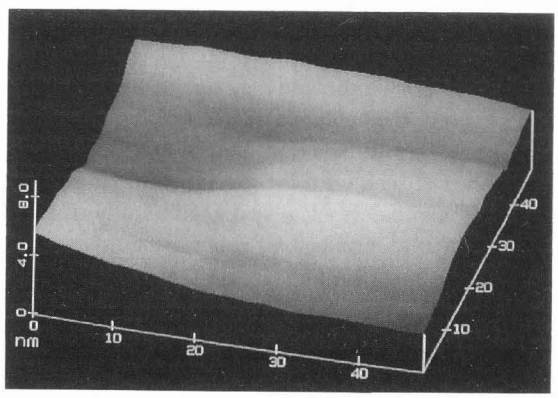

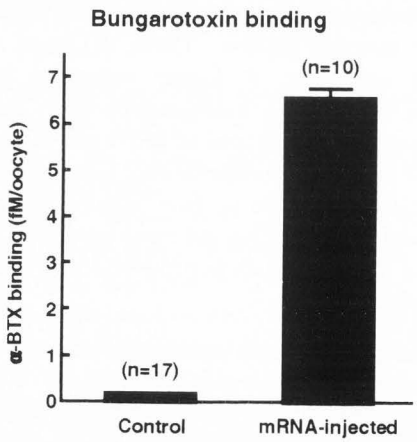

They were able to resolve rectangular unit cells (a=13.5 nm and b=8.2 nm) that comprise two trimers with central pore-like protrusions. Interestingly, they reported two conformations of these channels while imaging at a low force (0.1 nN) suggesting that AFM can be used to monitor conformational states of membrane proteins.

***Bacillus pertussis* porin**: Lal *et al.* (1993) were able to achieve molecular resolution on *B. pertussis* porins

Figure 9 on facing page

Figure 9: Molecular resolution AFM imaging of AChR expressed in *Xenopus* oocytes. After recording ACh sensitive electrical current in an oocyte, its vitelline membrane was manually removed for AFM imaging. The cell was cut into two halves and one half was imaged. Top left: Low magnification AFM image of the plasma membrane. A crack in the membrane is shown. The thickness appears to be ~13 nm, the predicted thickness of AChR spanning the plasma membrane. Middle left: High-resolution **low pass filtered** images of an oocyte expressing the mouse AChR channels, showing the irregular spacing of receptor clustering. Bottom left: High resolution image of a control oocyte not injected with any mRNA. Top right: Line graph of an image of a single AChR channel (~10.5 nm dia), showing the contour map of individual subunits and the central pore. The five subunits (~1-1.5 nm in dia) with a central pore like structure are shown. The protrusion of one unit is not apparent in the image. Middle right: ACh sensitive current measured in an oocyte after the AChR expression. The dose-dependent ACh sensitive current was reversible. Bottom right: α-bungarotoxin binding assay revealed a high level of AChR expression. The channel density calculated from AFM, electrophysiological, and pharmacological studies were comparable. For details see Lal and Yu, 1993.

---

which were packed in a quasi-rectangular order. These images also showed a lack of strong long range order, commonly observed for naturally occurring membranes and viewed by EM; indicating the molecular motion in a native environment and perhaps tip induced perturbations. In addition, molecular resolution surface topology of *B. pertussis* porins was obtained for the first time (Figure 7). The individual trimeric porins were visible. In a few cases on can see monomeric components that had pore like central depressions and several surrounding bead like protrusions, perhaps the ß-sheet folding of polypeptide.

Cholera-toxin B-oligomers: Yang *et al.* (1993), incorporated purified cholera toxin into synthetic phospholipid bilayers by covalent cross-linking. Imaging under an appropriate buffer they were able to obtain images of a pentameric structure at molecular resolution. The lateral dimension of individual subunits was comparable to that obtained by other methods, however the height of these units was significantly lower. It is not clear whether this reflects the partial embedding of protein in the lipid substrate and /or imaging force induced compression of the proteins.

Mou *et al.* (1995) have imaged isolated cholera toxin B-oligomers which were anchored to supported bilayers made of DPPC and POPG (Figure 8). Cholera toxin B-oligomers were seen to bind to the ganglioside in the fluid phase. Individual oligomers, their subunit organization, and few missing subunits were clearly resolved at a lateral resolution of ~1 nm. The image quality and resolution were comparable in both the fluid phase and the gel phase of the bilayer, suggesting that the bilayer fluidity did not introduce any significant perturbation during high resolution imaging. In addition, they were able to grow 2D arrays of B-oligomers directly on these model membranes without any special treatment. These studies suggest that isolated membrane proteins can be imaged with AFM without any significant chemical modifications such as cross-linking with the substrate.

Ca-ATPase: Lacapere *et al.* (1992) have imaged 3D crystals of Ca-ATPase which were reconstituted from 2D crystalline membranes isolated from sarcoplasmic reticulum vesicles. In their study, the lateral resolution was limited and they were not able to image crystal periodicity on the surface. However, the steps of membrane planes were measured which correspond to the unit cell spacings. While imaging under aqueous medium, they observed a significantly greater mobility on the surface, perhaps reflecting the intrinsic flexibility of layers of membrane sheets.

As the spectrum of AFM imaging is expanding, it is becoming clear that molecular resolution can be obtained on non-crystalline specimens in fluid medium. This opens a new avenue for the study of molecular structure of biological macromolecules such as ion channels and receptors that can be easily expressed in an appropriate expression system such as Xenopus oocyte, or simply isolated and anchored properly on a suitable substrate.

Whole cell plasma membrane and isolated organelles

AChR: Using the Xenopus oocyte expression system, nicotinic acetylcholine receptor (AChR) has recently been imaged (Lal and Yu, 1993) (Figure 9). Imaging whole and hemi oocytes whose vitelline membrane was removed showed a typical plasma membrane with thickness approaching 13 nm. This thickness (compared to a thickness of ~5.5 nm for a typical lipid bilayer) is consistent with the thickness of AChR spanning the plasma membrane which was predicted based on EM reconstruction (Unwin, 1993). Additionally, there was a noticeable step in the membrane indicating(?) the lipid leaflet interface, analogous perhaps, to images generated by freeze fracture EM. High resolution images on these membranes showed clusters of pentameric structures with a center to center spacing of 10-11 nm, close to the minimum center to center spacing of

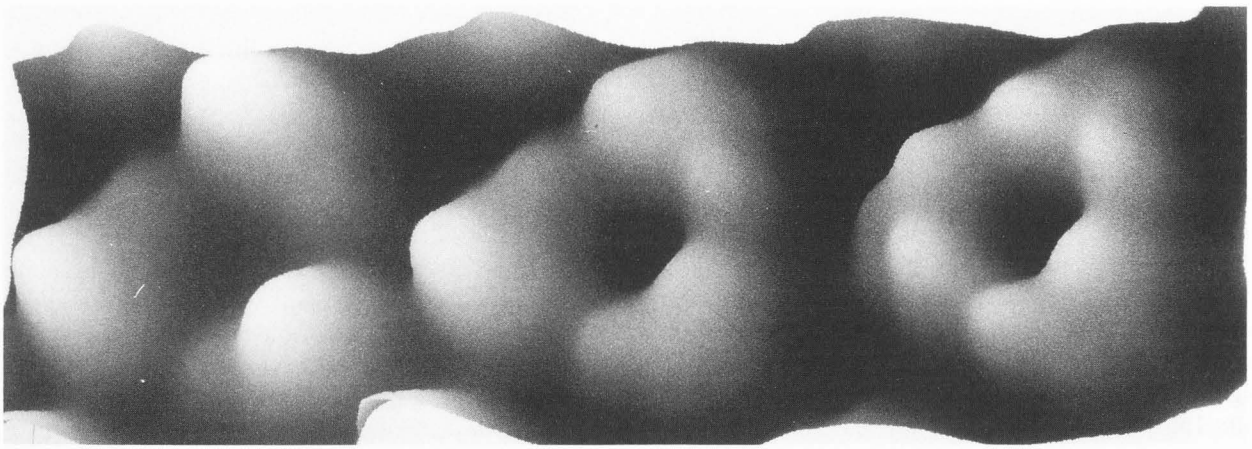

Figure 10: Force dependent conformational change of bacteriorhodopsin. Perceptive view (scale bar represents 2 nm) of the transition from native (left) to donut-shaped bacteriorhodopsin trimers (right). The central trimer is a composition of the left trimer recorded at 100 pN and the right trimer recorded at 300 pN. (For details, see Muller *et al.*, 1995).

---

about 9-10 nm for the 250 kD multisubunit AChR. The structure imaged shows three main protrusions, perhaps subunits from the membrane, and two minor protrusions, (perhaps other two subunits), and a pore like center depression. The angle between the two alpha subunits was ~128 degrees, in agreement with the reported value. The five subunit is consistent with that organization predicted from EM studies (Unwin, 1993). The height of these protrusions varied (0.7 ± 0.1 nm) but was significantly smaller than the previously reported value, which maybe accounted for by either tip induced flattening or drying of the sample.

Calcium channel: Haydon *et al.* (1994) have reported the localization of calcium channels on the calyx-type nerve terminal of the fixed chick ciliary ganglion in culture. These calcium channels were localized by imaging avidin-coated 30 nm gold particles which were incubated with biotinylated w-conotoxin GVIA. Calcium channels were clustered in low (~1 per μm^2) as well as high (55 per μm^2) density with an interchannel spacing of 40 nm. No molecular structure of individual calcium channels was reported possibly due to a low resolution commonly obtained while imaging intact cells. The interchannel spacing of 40 nm may reflect the spatial limitation due to the tagging with 30 nm gold particles. Also, individual calcium channels probably will be much smaller in diameter. Other membrane channels such as sodium and potassium channels and gap junctions are ~6-10 nm in diameter.

NPC: Isolated cellular organelles have been imaged with AFM. Oberleithner *et al.* (1994) have imaged nuclear pore complexes (NPC) in isolated and air dried nuclear surface of cultured kidney cells. These NPCs were ~134 nm in outer diameter with a central pore-like trough. NPCs were randomly distributed and their density increased from 7.4 to 9.8 per μm^2 in cells which were previously treated with aldosterone.

These studies of cells and cellular surfaces both fixed and unfixed, and imaged in dry or wet environment provides encouragement for undertaking studies for direct structure-function studies.

Structure-Function Studies

Significant advantages of AFM over conventional high resolution microscopy is that AFM allows imaging under an aqueous environment and AFM can be combined with other techniques for simultaneous or successive structure-function studies. Such potentials of AFM have just begun to be used for biological studies.

Lal and Yu (1993) reported a "single cell" experiment where electrical activity and surface images were obtained from *Xenopus* oocytes that were expressing AChR (Figure 9). Electrophysiological studies on the expressed oocytes revealed ACh sensitive current. Immunolabeling experiments on the expressing oocytes, by binding of AChR specific α-bungarotoxin, were also conducted in parallel. The receptor density calculated from AFM studies correlated well with the electrophysiological measurements and toxin binding, but the clustering of AChR was found to differ from the predicted uniform distribution of the expressed receptors as commonly assumed in electrophysiological studies. The density in the clusters was as high as seen in neuromuscular junctions. With further understanding and improvement in AFM imaging, it may not be long before when one can design whole cell-to-individual molecule experiment in a physiological environment.

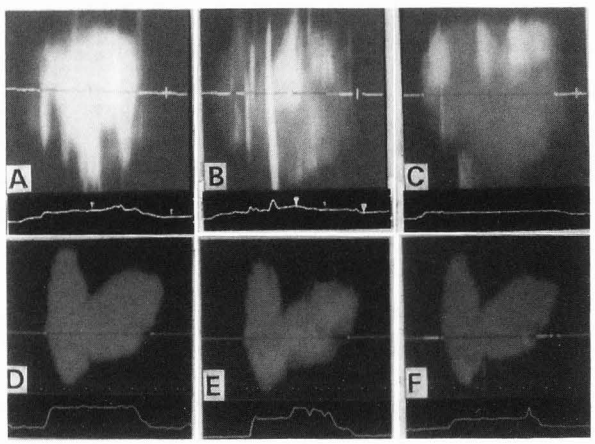

Figure 11: Comparison of force-dissection of heart (A, B, C) and liver (D, E, F) gap junctions. The top view images and thickness profiles along a line-cut perpendicular to the scan direction are shown for a series of scans at increasing forces of imaging. A, B, C: Heart gap junction. Imaging forces are 0.1 nN (A), 5.2 nN (B) and 11.6 nN (C), respectively. The thickness of the dissected single layer is reduced from ~21 nm to ~9 nm. The scan size is 875 x 875 nm^2. D, E, F: Liver gap junction. Imaging forces are 0.8 nN (D), 3.1 nN (E), and 10.1 nN (F), respectively. The thickness is reduced by half from ~15.5 nm to ~7 nm. The scan size is 1.5 x 1.5 μm. (for details, see Hoh *et al.*, 1991; Lal *et al.*, 1995b).

Bustamante *et al.* (1996) have reported correlative patch-clamp electrical recording and AFM of transcription factor IID (TFIID) interactions with the nuclear pore complex (NPC) isolated from kidney cells. The nuclei were fixed in glutaraldehyde after incubation with or without TFIID and ATP. Individual NPCs were imaged and a change in surface topology was apparent after treatment with TFIID as if the TFIID interaction was able to constrict the pore size. In a parallel set of experiments, they were able to show NPC unplugging accompanied by prolonged electrical current through the channel, perhaps reflecting the reopening of the channels.

Hörber *et al.* (1995) have combined AFM with patch-clamp technique in the same experiments and measured the electrical current in the excised membrane patches from *Xenopus* oocyte and attached to the patch pipette tip while imaging the surface topology with AFM. Notably, these membrane patches were significantly more stable and produced higher resolution images than imaging over a whole cell. Also, they were able to deform the membrane surface by applying pressure through the patch pipette and observed the lateral displacement of features. The resolution was limited to about 10 nm. Nevertheless, it shows the promises of direct structure-function studies of membrane structures and with further improvement it can be extended to molecular level.

Butt (1992) and Butt *et al.* (1993) have simultaneously imaged the 3-D structure of purple membrane, measured ion transport through the membrane, and examined the electrical properties of the membrane adsorbed onto a lipid monolayer. Dietz *et al.* (1991) have measured electric charge transfer through synthetic ultrafiltration membranes. And, Proksch *et al.* (1996) have simultaneously imaged the surface structure of nucleopore filters and measured electrical current passing across the filter through pores of different diameters. For these studies, they developed a combined scanning ion conductance microscope which can record electrical activity while imaging the 3D structure of various membranes.

Imaging force can be varied considerably during the experiments. Such feature has been used to nanomanipulate proteins and membrane structures (Florin *et al.*, 1994; Hoh *et al.*, 1991; Lal *et al.*, 1995b; Hörber *et al.*, 1995; Muller *et al.*, 1995a). Muller *et al.* (1995a) have elegantly reported two different conformations at the cytoplasmic surface of purple membranes (Figure 10). When the imaging force was reduced from ~300 picoNewton to 100 picoNewton, individual donut-shaped trimeric bacteriorhodopsin molecules transformed into units with three dominant protrusions.

Previously, Lal and his collaborators (Hoh *et al.*, 1991; Lal *et al.*, 1994,1995b) have shown that by a controlled increase in the imaging force it was possible to nanodissect the double bilayer gap junctions (Figure 11). Interestingly, it was also possible to obtain higher resolution on the membrane surface exposed after nanodissection (Hoh *et al.*, 1991,1993). Whether such enhanced resolution was due to some force-induced modulation or simply a function of the reduced extramembranous mass of gap junction polypeptides (connexins) need to be resolved.

Conclusion

The simple design and invariance to the operating environment allows AFM to be integrated with other techniques for correlational studies. The integration of the AFM and fluorescence microscope is one such exciting development (Hansma *et al.*, 1994b, Lal *et al.*, 1995a,b). Schmitt *et al.* (1992) have studied molecular recognition reactions at receptor-substrate interfaces using fluorescence, plasmon surface polaritons and AFM. Toledo-Crow *et al.* (1992) have combined near-field differential scanning optical microscope with AFM. Emerging technique of AFM based NMR imaging

(Rugar *et al.*, 1993) provides the most promising avenue of 3-D structural analysis of individual macromolecules without the need of crystallization and related complications. New cryo-atomic force microscope, developed by Shao and his collaborators (Han *et al.*, 1995) will provide a significant impetus for high resolution and even atomic resolution imaging of channels and receptors, both isolated and those present in cell membranes.

The studies of hydrated channels and receptors show potential for direct structure-function studies of these biological macromolecules that can be properly anchored, reconstituted and or expressed in a suitable expression system. As these membranes can be imaged under an appropriate buffer, it may be possible to observe short- and long-term molecular interactions with various ligands (e.g., antibodies, toxins, drugs).

Acknowledgments

Vacuolar ATPase was prepared and characterized by Drs. Kathleen Nolta and Ted Steck at the University of Chicago. I thank them for providing acidosomes and for their participation during the preliminary work related to vacuolar ATPase. The porin channel reconstitution and the lipid-protein interaction were carried out by Drs. Hoein Kim and Michael Garavito. I thank them for their effort and encouragement. I thank Dr. Z. Shao for providing images of cholera-toxins and Dr. D.J. Muller for providing images of bateriorhodopsins. Supported by the Cottage Hospital-Digital Instruments Special Research Award and the Alzheimer's Disease Program, Department of Health, California.

References

Arakawa H, Umemura K, Ikai A (1992) Protein images obtained by STM, AFM and TEM. Nature **358**: 171-173.

Binnig G, Quate CF, Gerber C (1986) Atomic force microscope. Phys Rev Lett **56**: 930-933.

Bustamante JO, Liepins A, Prendergast RA, Oberleithner H (1996) Patch-clamp and atomic force microscopy demonstrate transcription factor IID (TFIID) interactions with the nuclear pore complex. J Membr Biol **146**: 263-72.

Butt HJ (1992) Measuring local surface charge densities in electrolyte solutions with a scanning force microscope. Biophys J **63**: 578-582.

Butt HJ, Downing KH, Hansma PK (1990) Imaging the membrane protein bacteriorhodopsin with the atomic force microscope. Biophys J **58**: 1473-1480.

Butt HJ, Seifert K, Fendeler K, Bamberg E (1993) Characterizing solid supported membranes with the atomic force microscope. Biophys J **64**: A14.

Dietz P, Hansma PK, Herrmann K-H, Inacker O, Lehmann HD (1991) Atomic force microscopy of synthetic ultrafiltration membranes in air and under water. Ultramicroscopy **35**: 155-159.

Drake B, Gould SC, Weisenhorn AL, Hansma HG, Hansma PK, Quate CF, Prater CB, Albrecht TR, Cannell DS (1989) Imaging crystals, polymers, and processes in water with the atomic force microscope. Science **243**: 1586-1589.

Durbin SD, Carlson WE, Saros MT (1993) In situ studies of protein crystal growth by atomic force microscopy. J Phys D Appl Phys **26**: B128-132.

Florin E-L, Moy VT, Gaub HE (1994) Adhesion forces between individual ligand-receptor pairs. Science **264**: 415-417.

Han W, Mou J, Yang J, Shao Z (1995) Cryo atomic force microscopy: A new approach for biological imaging at high resolution. Biochemistry **34**: 8216-8220.

Hansma HG, Hoh JH (1994) Biomolecular imaging with the atomic force microscope. Annu Rev Biophys Biomol Struct **23**: 115-128.

Hansma PK, Cleveland JP, Radmacher M, Walters DA, Hillner P, Bezanilla M, Fritz M, Vie D, Hansma HG, Prater CB, Massie J, Gurley J, Elings V (1994a) Tapping mode atomic force microscopy in liquids. Appl Phys Lett **64**: 1738-1742.

Hansma PK, Drake B, Grigg D, Prater CB, Yasher F, Gurley G, Elings V, Feinstein S, Lal R (1994b) A new, optical-lever based atomic force microscope. J Appl Phys **76**: 796-799.

Haydon PG, Henderson E, Stanley EF (1994) Localization of individual calcium channels at the release face of a presynaptic nerve terminal. Neuron **13**: 1275-1280.

Hillner PE, Walters DA, Lal R, Hansma HG, Hansma PK (1995) Combined atomic force and confocal laser scanning microscope. J Micro Soc Am **1**: 123-126.

Hoh JH, Lal R, John SA, Revel JP, Arnsdorf MF (1991) Atomic force microscopy and dissection of gap junctions. Science **253**: 1405-1408.

Hoh JH, Sosinsky GE, Revel J-P, Hansma PK (1993) Structure of the extra-cellular surface of gap junction by atomic force microscopy. Biophys J **65**: 149-163.

Hörber JKH, Haberle W, Ohnesorge F, Binnig G, Liebich HG, Czerny CZ, Mahnel H, Mayr A (1992) Investigation of living cells in the nanometer regime with the scanning force microscope. Scanning Microsc **6**: 919-930.

Hörber JKH, Mosbacher J, Haberle W, Rupersberg JP, Sakmann B (1995) A look at membrane patches with a scanning force microscope. Biophys J **68**: 1687-1693.

Karrasch S, Dolder M, Schabert F, Ramsden J, Engel E (1993) Covalent binding of biological samples

to solid supports for scanning probe microscopy in buffer solution. Biophys J **65**: 2437-2446.

Kordylewski L, Saner D, Lal R (1994) Atomic force microscopy of freeze-fracture replicas of rat atrial tissue. J Microscopy **173**: 173-181.

Lacapere JJ, Stokes DL, Chatenay D (1992) Atomic force microscopy of 3-dimensional membrane-protein crystals - Ca-ATPase of sarcoplasmic reticulum. Biophys J **63**: 303-308.

Lal R, Kim H, Garavito RM, Arnsdorf MF (1993) Molecular resolution imaging of outer membrane channels reconstituted in an artificial bilayer. Am J Physiol **265**: C851-C856.

Lal R, Drake B, Blumberg D, Saner D, Hansma PK, Feinstein S (1995a) Imaging neurite outgrowth and cytoskeletal reorganization with an atomic force microscope: studies on PC12 and NIH3T3 cells in culture. Am J Physiol **269**: C275-C285.

Lal R, John SA, Laird DW, Arnsdorf MF (1995b) Heart gap junction preparations reveal hemiplaques by atomic force microscopy. Am J Physiol **268**: C968-C977.

Lal R, Yu L (1993) Molecular structure of cloned nicotinic AChR receptors expressed in *Xenopus* oocyte as revealed by atomic force microscopy. Proc Natl Acad Sci **90**: 7280-7284.

Lal R, John SA (1994) Biological application of atomic force microscopy. Am J Physiol **256**: C1-C21.

Mou J, Yang J, Shao Z (1995) Atomic force microscopy of cholera toxin B-oligomers bound to bilayers of biologically relevant lipids. J Mol Biol **248**: 507-512.

Muller DJ, Buldt G, Engel A (1995a) Force-induced conformational change of bacterio-rhodopsin. J Mol Biol **249**: 239-243.

Muller DJ, Shabert FA, Buldt G, Engel A (1995b) Imaging purple membranes in aqueous solutions at sub-nanometer resolution by atomic force microscopy. Biophys J **68**: 1681-1686.

Nolta KV, Padh H, Steck TL (1991) Acidosomes from *Dictyostelium*. Initial biochemical characterization. J Biol Chem **266**: 18318-18323.

Oberleithner H, Brinckmann E, Schwab A, Krohne G (1994) Imaging nuclear pores of aldosterone-sensitive kidney cells by atomic force microscopy. Proc Natl Acad Sci **91**: 9784-9788.

Ohnesorge F, Binnig G (1993) True atomic resolution by Atomic Force Microscopy through repulsive and attractive Forces. Science **260**: 1451-1456.

Paul JK, Nettikadan SR, Ganjeizadeh M, Yamaguchi M, Takeyasu K (1994) Molecular imaging of Na-K-ATPase in purified kidney membranes. FEBS Lett **346**: 289-294.

Proksch RA, Lal R, Hansma PK, Morse D, Stucky G (1996) Imaging the internal and external pore structures of membrane in fluid: tapping mode scanning ion conductance microscopy. Biophys J **71**: 2155-2157.

Rugar D, Yannoni CS, Sidles JA (1992) Mechanical detection of magnetic resonance. Nature **360**: 563-566.

Schabert FA, Henn C, Engel A (1995) Native *E coli* OmpF porin surfaces probed by atomic force microscopy. Science **268**: 92-94.

Schmitt FJ, Weisenhorn AL, Hansma PK, Knoll W (1992) Molecular recognition reactions at interfaces as seen by fluorescence, plasmon surface-polaritons and atomic force microscopy. Thin Solid Films **210**: 666-669.

Shroff S, Saner D, Lal R (1995) Dynamic micromechanical properties of contractile cells measured by atomic force microscopy. Am J Physiol **269**: C286-292.

Toledo-Crow R, Yang PC, Chen Y, Vaez-Iravani M (1992) Near-field differential scanning optical microscope with atomic force regulation. Appl Phys Lett **60**: 2957-2959.

Unwin N (1993) Nicotinic acetylcholine receptor at 9 A resolution. J Mol Biol **229**: 1101-1124.

Yang J, Tamm LK, Tillack TW, Shao Z (1993) New approach for atomic force microscopy of membrane proteins - the imaging of cholera toxin. J Mol Biol **229**: 286-290.

Yang J, Shao Z (1995) Recent advances in biological atomic force microscopy. Micron **26**: 35-49.

Discussion with Reviewers

R. Marchant: I think some attention should be given to various technical difficulties and imaging artifacts that are encountered when using AFM. Examples include thermal drift and friction effects that can effect the precision and reproducibility of measurements in all dimensions; the non-linear combination of the tip and specimen that cause significant broadening of lateral measurements, particularly for biomolecules that are taller than 1 nm; the effect of imaging forces on delicate biomolecules (an adverse example of "nano-dissection"); and the need for well characterized tips to account for anomalies seen in the images; drawbacks of the optical lever detection, sample preparation issues, and anomalies observed in images as a result of the feedback system, particularly at faster scanning rates.

Author: I agree with the reviewer that these points should be discussed in a balanced and broad review of the biological application of AFM. However, this manuscript is written primarily to provide the breadth and scope of imaging membrane channels and receptors. And as such, in addition to providing some new data (Figures 5 and 6), the available literature on imaging channels and receptors were summarized. For detailed

treatise of the technical limitations and difficulties, readers can always refer to several current review articles such as Lal & John, 1994, Hansma & Hoh, 1995, Yang & Shao, 1995.

J. Zasadzinski: What limits the resolution with contact mode AFM? Will non-contact modes - tapping, adhesion etc. or lateral foerce provide higher resolution or other important data?
Author: The scope of the present manuscript is limited to providing examples of AFM applications to channels and receptors. The reviewer's question is better answered in the above mentioned review articles and other cross references.

J. Zasadzinski: What are the major benefits to AFM studies of membrane proteins over cryo-electron microscopy? Are there certain systems that just cannot be done with TEM that can be examined by AFM? Are there systems in which the AFM resolution is superior to the TEM?
Author: There are several advantages of AFM imaging over EM. (a) The signal to noise ratio in AFM is high enough that one can view micro-details in even single channel and receptors. For similar information in EM studies, one need to average information from a large number of channels and receptors which are in a crystalline order; (b) The AFM images contain a greater detail of the surface topography which is an essential information about membrane proteins which has a large portion not embedded in the lipid bilayer. For example, heart gap junctions has a large cytoplasmic domain which prevents any high resolution structural information.

J. Zasadzinski: How important is the environment or the substrate in the protein conformation? Is the problem with resolution more that the protein is moving over the time scales of the images, thereby blurring the images? What are the benefits to such kinetic information that obviously cannot be determined from fixed or frozen material?
Author: Again this problem is well discussed in the several recent review articles cited above. A major advantage of AFM imaging is that, since it images hydrated specimen, it allows for real-time dynamic studies of protein conformations. This is still a new domain of AFM application and need to be further developed. The temporal resolution in an AFM images depends on several factors including the image size, spatial resolution and protein mobility. In general, slow lateral movement of small proteins can be followed in real-time (Thomson *et al.*, 1996). At present time, the rotational motion of protein molecules are too fast to be tracked in AFM imaging.

Additional Reference

Thomson NH, Fritz M, Radmacher M, Cleveland JP, Schmidt CF, Hansma PK (1996) Protein tracking and observation of protein motion using atomic force microscope. Biophys J **70**: 2421-2431.